*metals*

MDPI

*Article*

# Influence of a Pronounced Pre-Deformation on the Attachment of Melt Droplets and the Fatigue Behavior of Laser-Cut AISI 304

**André T. Zeuner [1,*], Thomas Wanski [1], Sebastian Schettler [2], Jonas Fell [3], Andreas Wetzig [2], Robert Kühne [2], Sarah C. L. Fischer [4] and Martina Zimmermann [1,2]**

[1] Institute of Materials Science, Technische Universität Dresden, 01069 Dresden, Germany
[2] Fraunhofer Institute for Material and Beam Technology IWS, 01277 Dresden, Germany
[3] Department of Materials Science and Engineering, Saarland University, 66123 Saarbrucken, Germany
[4] Fraunhofer Institute for Nondestructive Testing IZFP, 66123 Saarbrucken, Germany
* Correspondence: andre_till.zeuner@tu-dresden.de

**Abstract:** Laser cutting is a suitable manufacturing method for generating complex geometries for sheet metal components. However, their cyclic load capacity is reduced compared to, for example, milled components. This is due to the influence of the laser-cut edge, whose characteristic features act as crack initiation sites, especially resolidified material in the form of burr and melt droplets. Since sheet metal components are often formed into their final geometry after cutting, another important factor influencing fatigue behavior is the effect of the forming process on the laser-cut edge. In particular, the effect of high degrees of deformation has not yet been researched in detail. Accordingly, sheets of AISI 304 were processed by laser cutting and pre-deformed. In the process, $\alpha'$-martensite content was set to be comparable despite different degrees of deformation. It was found that deformation to high elongations caused a large part of the melt adhesions to fall off, but those still attaching were partially detached and thus formed an initial notch for crack initiation. This significantly lowered the fatigue strength.

**Keywords:** laser cutting; fatigue behavior; melt adhesion; resolidified material; detachment; notch; micro-computed tomography analysis



**Citation:** Zeuner, A.T.; Wanski, T.; Schettler, S.; Fell, J.; Wetzig, A.; Kühne, R.; Fischer, S.C.L.; Zimmermann, M. Influence of a Pronounced Pre-Deformation on the Attachment of Melt Droplets and the Fatigue Behavior of Laser-Cut AISI 304. *Metals* **2023**, *13*, 201. https://doi.org/10.3390/met13020201

Academic Editor: Antonio Riveiro

Received: 21 December 2022
Revised: 13 January 2023
Accepted: 17 January 2023
Published: 19 January 2023



## 1. Introduction

Laser beam cutting is a highly flexible and precise process capable of cutting a wide range of industrially relevant materials. The cut is realized by the energy of the laser beam, whereby molten material is expelled by process gas. This manufacturing process offers a number of advantages. Since there is no tool-to-workpiece contact, tool wear is avoided. In addition, no special tools are required for different component geometries or materials, which saves retooling time and reduces the required storage capacity. Laser cutting is, in particular, beneficial for the processing of materials that are difficult to mechanically process, such as titanium alloys or stainless steel. Despite the exceptional mechanical properties of these materials they are easily cut by laser beam cutting due to contactless processing [1,2].

The metastable austenitic stainless steel AISI 304 is a very commonly used sheet metal to which the scenario described above applies. AISI 304 is used in different industries such as chemistry, construction, energy, food, medicine, mechanical engineering, or mobility. For the last two fields of application, cyclic loading is common, for example, in the case of the exhaust gas system of automobiles. The wide field of application results from the advantageous properties of high strength, high ductility, and good corrosion resistance of AISI 304. The latter can be attributed to high chromium content and the face-centered cubic crystal lattice [3–5].

The mechanical behavior of AISI 304 is linked to a complex microstructural evolution which is called martensitic transformation. The martensitic transformation can be

thermal, stress, or deformation induced, whereby deformation-induced martensitic transformation has the highest significance for industrial application. This is the transformation of face-centered cubic γ-austenite into body-centered cubic α'-martensite under plastic deformation. It may incorporate the intermediate step of forming hexagonal close-packed ε-martensite [6–11]. For the mechanical properties, α'-martensite is particularly important because it has higher strength and hardness than γ-austenite [12–14].

Martensitic transformation is one factor why machining AISI 304 is challenging, which is a factor why machining by laser can be economically attractive [15]. However, studies on laser-cut materials showed that the fatigue limit is significantly reduced compared to milled or polished material; punched material achieves similar fatigue limits [16–18]. The reason for this is the notch effect of the re-solidified material, which is formed by the solidification of molten material on the melt ejection side of the sheet metal during laser cutting. Removing melt droplets slightly increases fatigue strength. However, pores in the re-solidified material adhering to the cutting edge act as crack initiation sites. Therefore, fatigue strength is still inferior compared to a classical mechanical subtractive machining process [19].

In a previous study, the influence of laser-cutting parameters and a subsequent pre-deformation on the fatigue behavior of laser-cut AISI 304 was investigated [20]. It was shown that depending on laser-cutting parameters, a pre-deformation can cause the detachment of melt droplets. This had a direct influence on the fatigue strength achieved. Laser-cutting parameters that realized melt droplets with a high tendency to detach during subsequent deformation resulted in higher fatigue strength. This is an important factor for the application of laser-cut sheet metal components, which subsequently have to be formed to the final component geometry. However, this detachment effect was only investigated in fatigue tests for amounts of pre-deformation below 30% strain. A comparison of different amounts of deformation showed that a large proportion of the melt droplets had already detached at up to 20% strain, while no significant additional detachment effect was achieved for deformation of up to 50% during tensile testing. The result of this investigation is depicted in Figure 1 for two batches. At this point, the question arises as to how the melt adhesions behave under further plastic deformation significantly above the investigated deformations of less than 30%. After all, significantly higher forming degrees can be achieved in industrial forming steps.

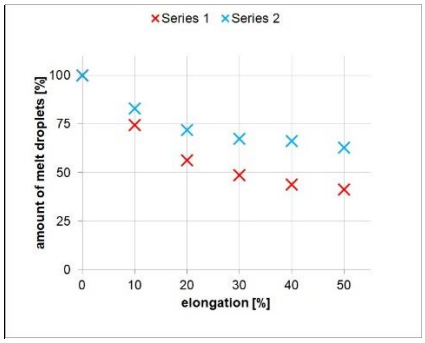


**Figure 1.** Detachment behavior of melt droplets caused by pre-deformation [20].

In summary, the pre-deformation of a laser-cut AISI 304 has several effects on fatigue behavior. On the one hand, work hardening as well as deformation-induced α'-martensite transformation leads to a strengthening of the material, which leads to an increase in cyclic load-bearing capacity. On the other hand, melt droplets can detach from the workpiece due to weak attachment. This reduces the notch effect and also increases fatigue strength. However, a second mentioned was only investigated in fatigue tests for pre-strains below 30%.

Since degrees of deformation significantly above 30% strain can be achieved in many applications of formed sheet metal components, the objective of this study was to investigate the effect of high grades of pre-deformation on laser-cut AISI 304 material and its

influence on fatigue behavior. As the attachment of melt droplets has been found to be an important factor for deformation-induced detachment as well as fatigue behavior, it was particularly important to investigate whether and to what extent the attachment to the base material changes in the case of high degrees of deformation.

## 2. Material and Methods

### *2.1. Specimen Preparation*

The fatigue behavior of laser-cut AISI 304 is sensitive to a number of influencing variables, some of which have already been described in the first section. Accordingly, it was important that all specimens were manufactured from the same sheet metal, received the same pre-treatment, and were cut on the same laser-cutting machine with the same cutting parameters. The chemical composition and mechanical properties of the investigated 2 mm thick AISI 304 steel sheet are shown in Tables 1 and 2, respectively.

**Table 1.** Chemical composition of AISI 304 provided by the manufacturer.

| Element | C | S | P | Mn | Si | Cr | Ni | N | Fe |
|---|---|---|---|---|---|---|---|---|---|
| wt-% | 0.016 | 0.001 | 0.036 | 1.90 | 0.36 | 18.2 | 8.1 | 0.01 | Bal. |

**Table 2.** Mechanical properties of AISI 304 provided by the manufacturer.

| Yield Strength/MPa | Tensile Strength/MPa | Elongation at Break/% |
|---|---|---|
| 275 | 620 | 54 |

Another measure was the heat treatment of the sheet material before laser cutting to ensure homogeneous phase distributions and properties. Therefore, the material was heat treated at 1363 K for 1 h and cooled fast in moving air for complete austenitization and recrystallization, which eliminates the rolling texture. Thus, influences from the rolling process could be excluded in the following investigations. Subsequently, a laser-cutting machine with a TruDisk 5001 disk laser of the company Trumpf (Ditzingen, Germany) was used. All specimens were produced with the same processing parameters, which are summarized in Table 3. Here, $f_{coll}$ stands for collimation length, $f_{foc}$ for focal length, $d_{nozzle}$ for nozzle diameter, $P_L$ for laser power, $v_f$ for feed rate, $d_z$ for focal position, $d_s$ for stand-off distance, $p_{gas}$ for gas pressure, $\lambda_L$ for laser wavelength, $M^2$ for beam quality factor, and $d_f$ for focus diameter. Nitrogen was used as a process gas.

**Table 3.** Laser-cutting parameters.

| $f_{coll}$/mm | $f_{foc}$/mm | $d_{nozzle}$/mm | $P_L$/kW | $v_f$/m·min$^{-1}$ | $d_z$/mm | $d_{ns}$/mm | $p_{gas}$/bar | $\lambda_L$/µm | $M^2$ | $d_f$/µm |
|---|---|---|---|---|---|---|---|---|---|---|
| 100 | 150 | 2.3 | 3 | 16.5 | 0 | 0.8 | 11 | 1.03 | 13.0 | 192 |

### *2.2. Examination of Melt Droplets by Micro-Computed Tomography*

The central question of how the bonding of melt droplets to the base material changes at high degrees of deformation was investigated in detail. For this reason, high-resolution micro-computed tomography (µCT) was chosen as the method of investigation so that 3D information could be generated. Due to the high density of the material investigated, the material volume must be small for this type of investigation. Accordingly, Figure 2 shows the used specimen geometry with a bridge volume of 2 mm$^3$, which was deformed to a local strain of 44% in the bridge close to the ultimate tensile strength of the specimens. The deformed bridge was cut out of the specimens and examined by µCT. Non-deformed specimens were examined for comparison.

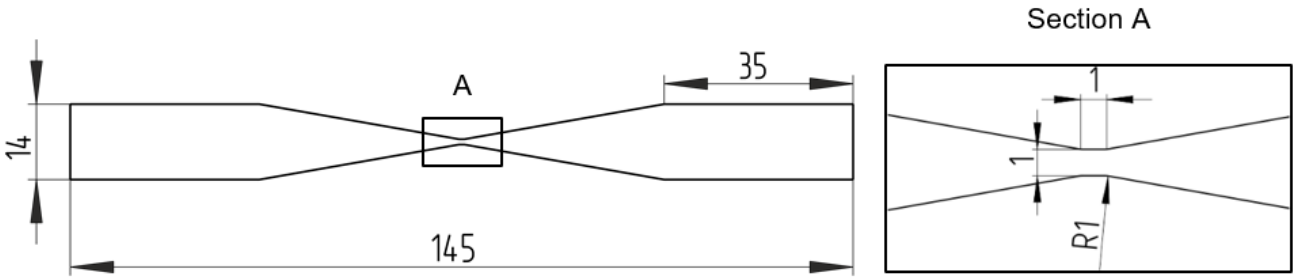


**Figure 2.** Specimen geometry for pre-deformation and µCT examinations made of 2 mm thick AISI 304 steel sheet with given dimensions in mm. Test region is shown magnified.

Micro-computed tomography was performed with a custom-built X-ray system at Fraunhofer IZFP, Saarbrücken, equipped with a micro-focus tube and a 4 k pixel detector. For the µCT measurement, 1600 projections over 360° were acquired with a tube voltage of 220 kV and a tube power of 100 Watt. A voxel size of approximately 2 µm could be reached. Volume reconstruction was carried out simultaneously with a custom reconstruction algorithm. Sectional planes showing the connection to the base material were then examined from this.

### *2.3. Fatigue Testing*

The effect of large degrees of deformation of laser-cut sheets examined by the µCT studies on fatigue behavior was another focus of the investigations presented. For fatigue testing, the specimen geometry in Figure 3 was used. For this purpose, a series of specimens with a deformation of 28% strain was investigated, as was done in a previous study [20]. A second series of specimens underwent a deformation of 44% strain, as did the specimens in the µCT study.

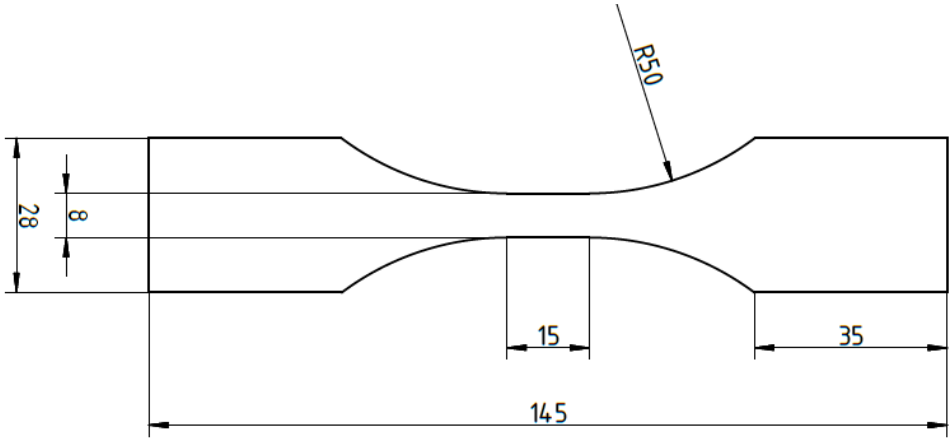


**Figure 3.** Specimen geometry used for tensile and fatigue testing made of 2 mm thick AISI 304 steel sheet with given dimensions in mm.

However, in order for these two series of specimens with different amounts of strain to be comparable, it was necessary to ensure that similar α'-martensite content was present in both series of specimens after pre-deformation. Otherwise, the specimen series with the higher α'-martensite content would already exhibit a higher cyclic load capacity due to the strengthening effect of α'-martensite. Accordingly, tensile tests to examine the influence of the deformation parameters strain, strain rate, and temperature on the deformation-induced martensitic transformation behavior were carried out for the given chemical composition and specimen geometry first. Therefore, a tensile testing machine from the company ZwickRoell (Ulm, Germany) and a climate chamber from the company mytron (Heilbad

Heiligenstadt, Germany) were used. In addition, a Feritscope from the company Fischer was used to measure the transformed α′-martensite content during the test. The calibration was carried out according to [21]. Using this test setup, tensile tests were performed at laboratory conditions (298 K), 273 K, 258 K, and 243 K. At each temperature, tests were performed at strain rates of 10 mm/min, 1 mm/min, and 0.1 mm/min achieved in the bridge of the specimens, respectively. Three samples were tested for each deformation state of temperature and strain rate. The results of this preliminary investigation are shown in Figure 4. Here the α′-martensite volume fraction $M_V$ is plotted against temperature and stress.

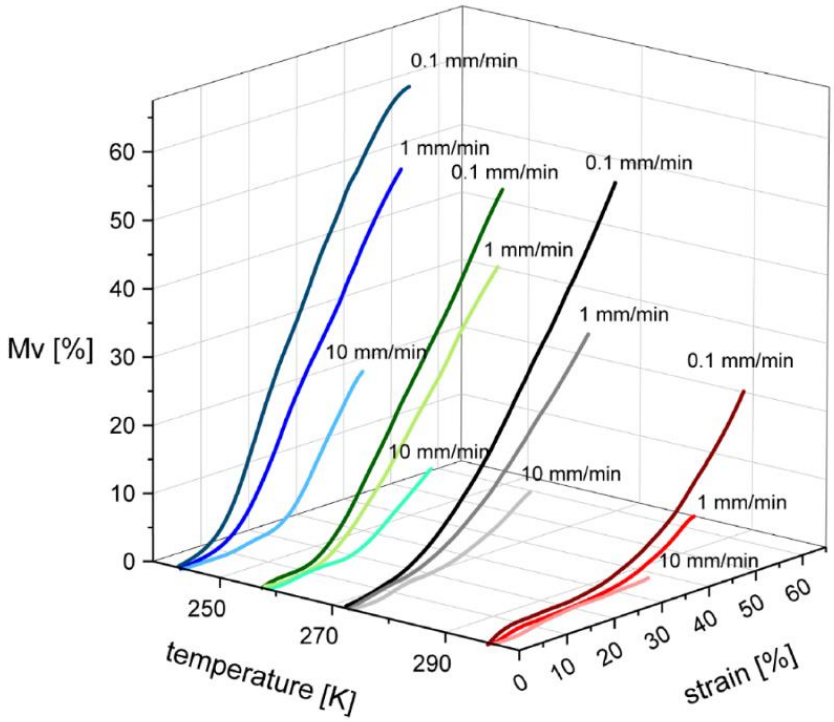


**Figure 4.** Relationship among ambient temperature, strain, strain rate, and α′-martensite volume fraction (Mv) for the chemical composition of AISI 304.

Based on tensile test results, two deformation regimes were selected that resulted in comparable α′-martensite contents, see Table 4. At both conditions, 15 specimens each were manufactured to investigate fatigue behavior. The first series of specimens were deformed at 298 K up to 44% and the second series of specimens were deformed at 273 K up to 28%, and they are accordingly referred to as 298K-44% and 273K-28%, respectively, in the remainder of this paper.

**Table 4.** Designation of specimen series, ambient temperature during pre-deformation, strain, strain rate, and number of specimens used to characterize fatigue strength.

| Series Name | Temperature/K | Strain/% | Strain Rate/mm/min | α′-Content/% | No. of Samples |
|---|---|---|---|---|---|
| 298K-44% | 298 | 44 | 1 | $10 \pm 2$ | 15 |
| 273K-28% | 273 | 28 | 1 | $10 \pm 2$ | 15 |

To investigate fatigue behavior, a Gigaforte testing machine from the company Russenberger Prüfmaschinen (Neuhausen am Rheinfall, Switzerland) was used. This machine realizes test frequencies of about 1 kHz. AISI 304 heats adiabatically under cyclic loading and therefore has to be cooled sufficiently [22,23]. Pre-deformed specimens already showed significantly reduced adiabatic heating compared to non-deformed AISI 304. Additionally,

cooling by means of a vortex tube was used and a stress ratio R of 0.5 was selected. The lower stress amplitudes compared to R of −1 or 0.1 resulted in a further significant reduction in adiabatic heating at high test frequencies. The combination of these actions ensured that the specimens did not exceed a temperature of 303 K during fatigue testing, which was monitored with a pyrometer. The tests were carried out to at least $10^8$ load cycles in order to be counted as a run-out. The procedure was in accordance with DIN 50100 (2016) [24], which describes a method to statistically determine fatigue strength by selecting the stress amplitude depending on the result of the previously tested sample (break or run out). This method allows an evaluation of the stress amplitude with a 50% failure probability, which is used as a characteristic value for the discussion of fatigue strength. A change in resonance frequency Δf of 2 Hz was applied as a criterion to stop fatigue testing, indicating technical crack initiation. Subsequently, fracture surface analyses were performed using a scanning electron microscope (SEM) JSM-6610LV of the company JEOL (Tokyo, Japan) to determine the location of crack initiation.

## 3. Results and Discussion

### *3.1. Effect of High Pre-Strains on the Bonding of Melt Droplets to the Base Material*

Since the pre-deformation was performed after cutting, the laser-cut edge was also deformed. The deformed laser-cut edges were examined by light microscopy and are shown exemplarily in Figure 5 for the conditions as cut (a) and pre-deformed to 28% strain (b). Comparing the two figures, the detachment phenomenon, which has been described in past work [20], due to plastic pre-deformation was again evident at the lower sheet edge.

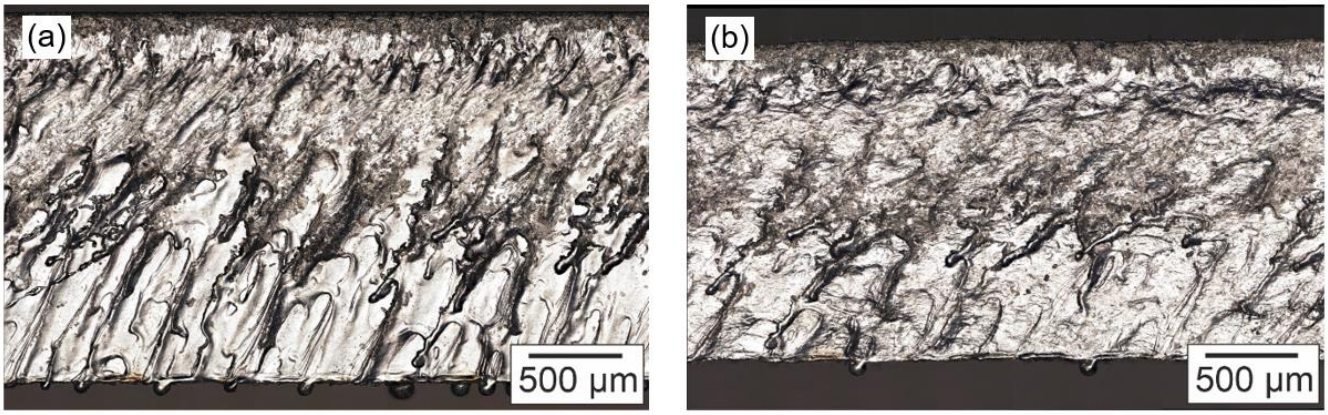


**Figure 5.** Top view of the laser-cut edge. (**a**) As cut, (**b**) Pre-deformed (ε = 28%).

Figures 6 and 7 show the results of the µCT examination. Here, slices of exemplary reconstructed melt droplets are shown for the two conditions as-cut and pre-strained to 44% highlighting the bonding condition on different observation planes, respectively. The images are to be understood in such a way that the labels above the images represent the depth of observation. In this case, surface means that the surface of the laser-cut edge—to the underside of which the melt droplet is attached—was observed. In the case of the label 36 µm, the observation plane was shifted 36 µm from the surface of the laser-cut edge into the sheet material. The melt droplet of the non-deformed sample in Figure 6 showed strong adherence to the base material, i.e., complete attachment to the base material was observed for the entire melt droplet volume. Opposite to the non-deformed sample, weak adherence of the melt droplet of the pre-deformed specimen can be clearly seen in Figure 7. Only at the surface was the droplet bonded to the base material. At a depth of 36 µm, the reconstructed slice already showed a large gap. This gap increased with greater observation depth to the surface of the laser-cut edge. At 88 µm, the melt droplet did not show a bond to the base material at all. This means that the melt droplet adhered only to the outer edge of the sheet and otherwise no longer had any bond to the base material. These results

indicate that the partial detachment created a notch between the melt droplet and the base material, which could be detrimental to the fatigue strength of the material at high levels of pre-deformation.

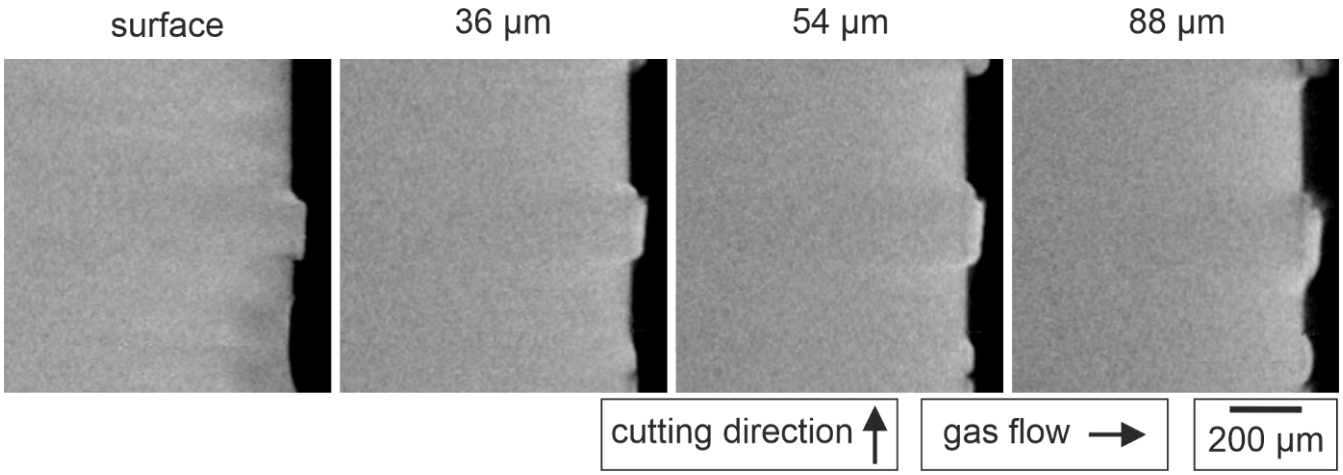


**Figure 6.** Selection of observation planes of the same re-solidified material droplet in the as-cut condition at different observation depths starting from the surface of the laser-cut edge.

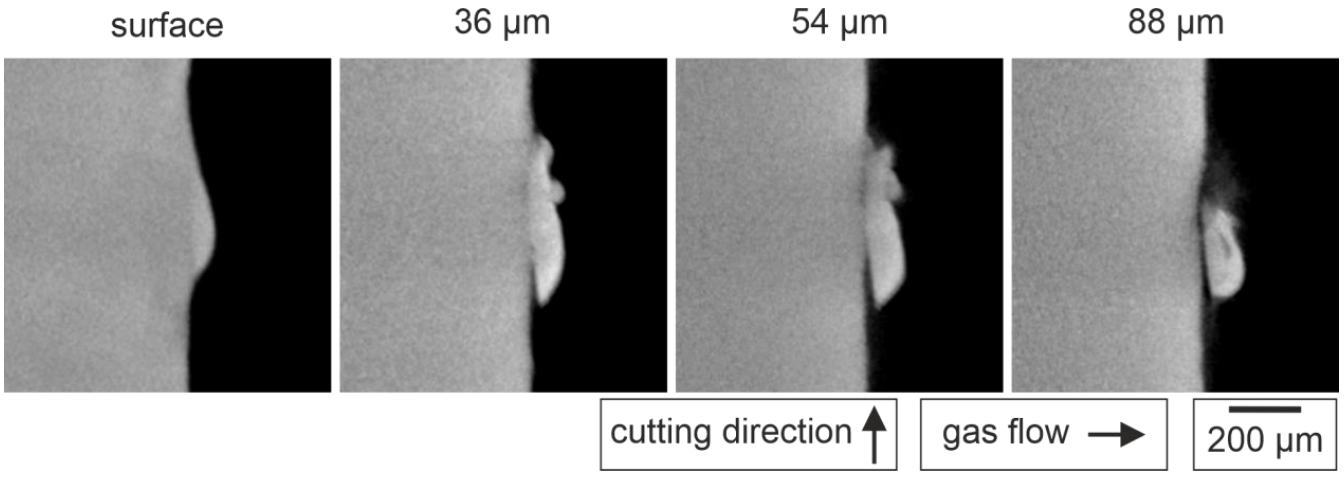


**Figure 7.** Selection of observation planes of the same re-solidified material droplet in the pre-deformed condition (44%) at different observation depths starting from the surface of the laser-cut edge.

### *3.2. Effect of High Pre-Strains on Fatigue Behavior*

The results of fatigue testing are shown in Figure 8, where stress is plotted over the number of load cycles in a S-N-diagram. It can be seen that the fatigue behavior of the tested specimen series differed significantly from each other. The highest stress levels were reached by the sample series 273K-28% (i.e., pre-deformed at 273 K and a strain of 28%). The fatigue strength for 50% failure probability at $10^8$ load cycles was 170 MPa according to DIN 50100.

On the contrary, sample series 298K-44% only showed a fatigue strength for a 50% failure probability of 145 MPa. Additionally, the measured values for load cycles until failure scattered considerably more. The failure of a specimen was even observed shortly before reaching $10^8$ load cycles.

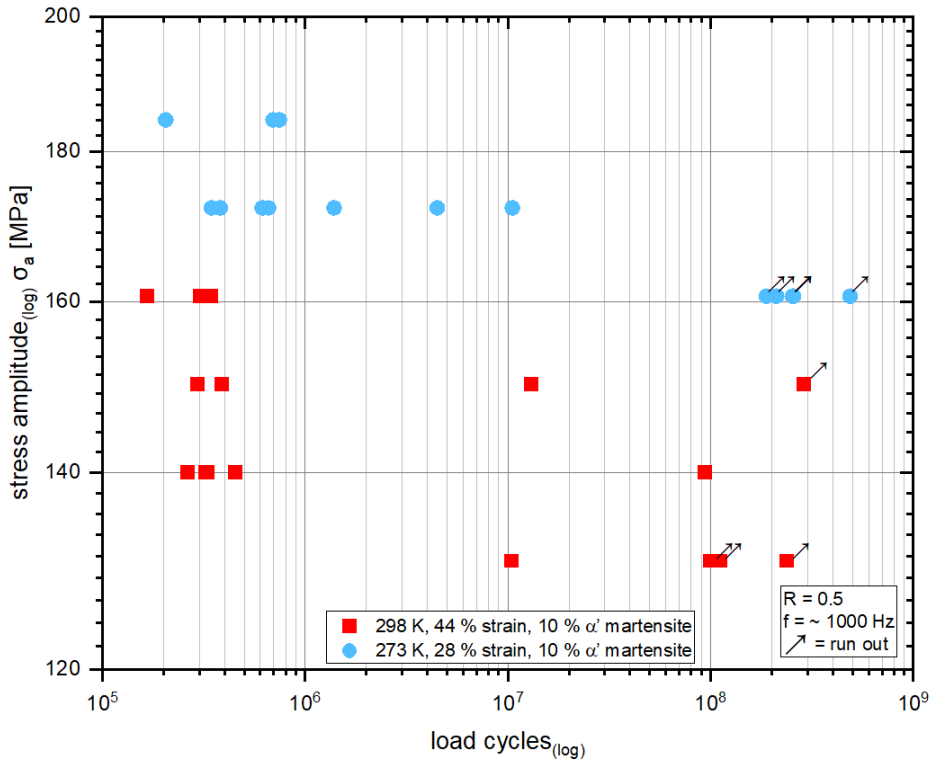


**Figure 8.** S-N diagram of fatigue tests on laser-cut AISI 304.

Following the fatigue tests, the fracture surfaces of all specimens were examined by SEM. It was observed consistently for all specimens that the location of crack initiation was at the melt ejection site of the laser-cut edge where molten material had re-solidified. In the case of the 298K-44% sample series, it was observed that the crack initiation site showed a characteristic feature with a smooth surface. This characteristic feature is shown in Figure 9, where in the case of (a), the fracture surface is shown from the top view. Figure 9b shows the specimen rotated by 45°. In this view, the sharp interface is visible between the smooth surface and the fatigue crack that propagated from this interface into the specimen volume. In the case of the specimen series 273K-28%, this observation was not made. For this sample series, the location of crack initiation is shown representatively in Figure 9c,d in the same way as for the 298K-44% sample series. It can be observed that the fatigue crack started in the outermost corner of the re-solidified material. A specific feature that served as crack initiation as was the case for 298K-44% is not identifiable here.

Through the previous investigations, it was hypothesized that the resolidified material was strongly deformed at the laser-cut edge, melt adhesions (partially) detached, and this led to a severe, crack-like notch for introducing premature fatigue crack growth. To support this argument, 44% of pre-deformed but non-fatigued specimens were re-examined by SEM. It was observed that the melt adhesions have a melt inflow, which remained at the laser-cut edge. This can be seen in Figure 10. This melt inflow showed a smooth surface similar to the crack-initiating feature in Figure 9a,b. Hence, it can be assumed that fatigue crack propagation indeed started at a notch-like partial detachment of a melt adhesion. Contrary to Figure 10, the melt adhesion itself is not visible in Figure 9, as it fell off either due to pre-deformation or during fatigue loading.

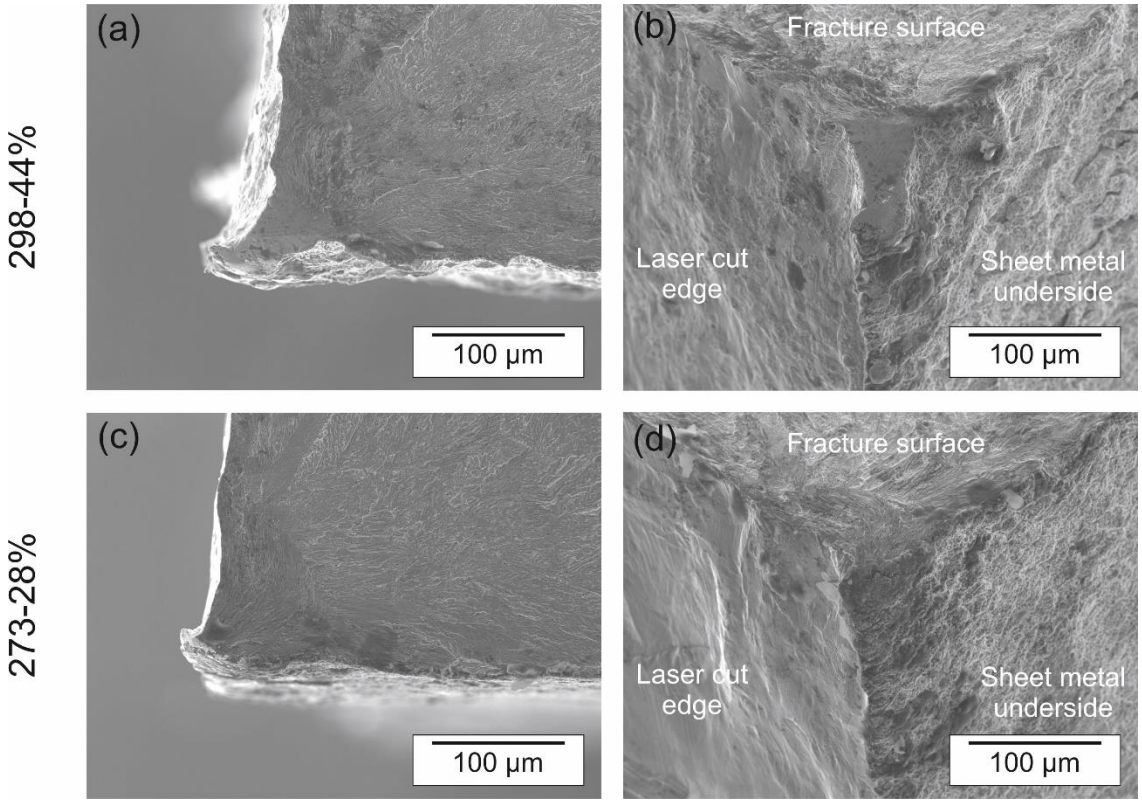


**Figure 9.** Selection of fracture surfaces captured by SEM. (**a**) 298K-44%, top view, (**b**) 298K-44%, 45°-perspective view, (**c**) 273K-28%, top view, (**d**) 273K-28%, 45°-perspective view.

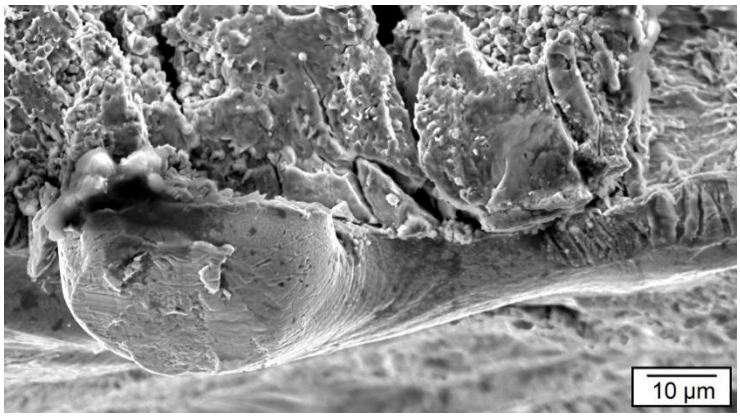


**Figure 10.** SEM detail image of a melt adhesion showing a melt inflow with a smooth surface, similar to the crack initiation site of the fracture surface for a sample pre-deformed to 44% elongation and subsequently fatigued.

In summary, both series 298K-44% and 273K-28% were manufactured from the same sheet, laser cut with the same parameters, and ultimately pre-deformed in a way that they had comparable $\alpha$'-martensite content in the base material. Their main difference can be found in the amount of pre-strain introduced. In the end, they showed clear differences in their fatigue behavior. When pre-forming, a significantly large number of melt droplets fell off the laser-cut material within the first 20% elongation, as was shown in previous work [20]. After that, the number of melt droplets decreased marginally. As soon as high elongations in a range close to the tensile strength were reached, it was observed by means of µCT, that the remaining melt droplets no longer detached completely, but

partially. Due to only partial bonding to the base material, a crack-like notch formed, see Figure 7, which served as a crack initiation site during the cyclic loading in the fatigue test. This assumption is supported by the smooth features of the fracture surfaces in Figure 9a,b as well as Figure 10, which could not be found in Figure 9c,d. For a better understanding of the significance of the partial detachment of the melt adhesion, the particular mesoscopic features of the pre-damage introduced through the combination of laser cutting and subsequent pre-deformation are schematically drawn in Figure 11.

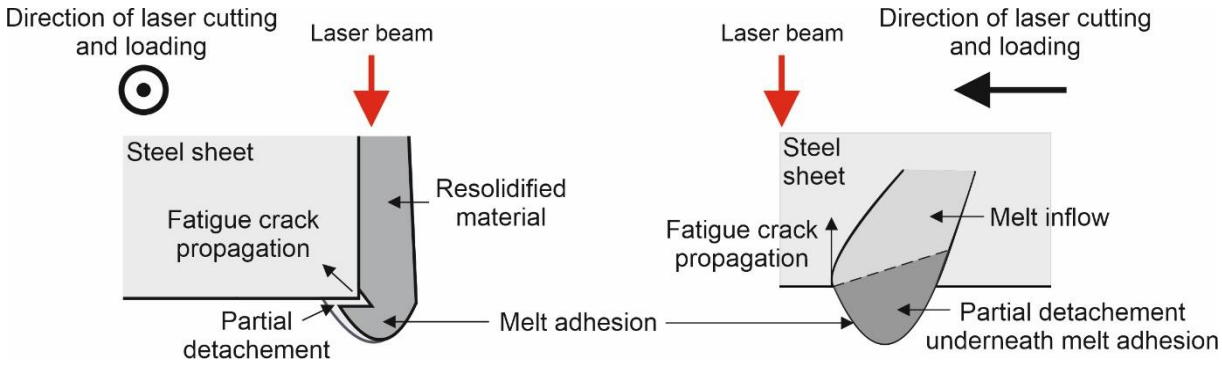


**Figure 11.** Schematic drawing for partial detachment of melt adhesions on strongly deformed laser-cut edges.

The fatigue test results in Figure 8 showed that this pre-damage due to laser cutting and pre-forming to high degrees of deformation can lead to significantly reduced fatigue strength and very late failures close to $10^8$ load cycles. However, both series have in common that the crack initiation took place in the lower outermost corner of the laser-cut edge at the re-solidified material, i.e., melt droplets. The significant difference in pre-strain in the base material did not change this situation. This underlines the central importance of the re-solidified material for the fatigue behavior of laser-cut materials. In this case, it was discovered that the partial detachment of melt droplets and the associated notch formation leads to crack initiation under cyclic loading and hence, has a significant influence on the cyclic strength. Through a careful selection of the laser-cutting parameters alone, the cyclic strength of AISI 304 can already be influenced, as could be shown in [20]. A subsequent pre-deformation—as would be typical for a car body application—will have an additional effect on the fatigue strength. For laser-cut sheet metals, this pre-deformation effect cannot solely be explained by the two strengthening mechanisms, namely strain-hardening and deformation-induced α′ martensite formation. These purely microstructure-related mechanisms have already been investigated comprehensively in the past, see e.g., [25–28]. In the study presented, the higher pre-deformation should have resulted in a beneficial effect due to an increased strain-hardening since the α′ martensite volume fraction was kept constant. However, the higher pre-deformation, in fact, caused a pronounced decrease in the cyclic strength. Fractographic analyses and µCT examinations showed that the effect of dross formation and its partial detachment excel the microstructural strengthening effects on fatigue behavior. From this, it can be deduced that in the case of laser cutting and subsequent forming of AISI 304, a reliable prediction of the fatigue strength strongly depends on a comprehensive understanding of the process–history interactions and their effect both on microstructural changes as well as mesoscopic notch effects.

In previously typical applications for laser cutting, a "clean and accurate" cutting edge is considered as one of the decisive evaluation criteria. Interdependencies between remaining re-solidified material after processing and the thermal impact on the materials' microstructure are of minor importance. However, in the case of laser-cut parts subjected to cyclic mechanical loading, this no longer holds. As is well known from former very high-cycle fatigue research, the influence of isolated micro-notches plays a decisive role in fatigue behavior with an increasing number of cycles. Transferring this observation to

the particularly rugged surface relief at the laser-cutting edge, crack initiation will most likely occur at a single, most detrimental, and therefore, failure-relevant micro-notch. The stochastic distribution of the mesoscopic geometrical characteristics of the rugged surface relief of the laser-cut surface is practically not determinable. Nonetheless, the results presented allow for an evaluation of the interaction between the material's microstructural and laser-cut surface characteristics in dependence on the process–history. It could be shown that the effect of dross formation and its partial detachment excel the microstructural strengthening effects.

## 4. Conclusions

By means of μCT investigations on laser-cut and highly pre-formed specimens, it could be shown that this process–history leads to the partial detachment of melt droplets, which causes notch formation on a mesoscopic scale. Fatigue tests up to $10^8$ loading cycles were conducted, since in this particular regime localized discontinuities define the fatigue behavior. Two deformation states (28 and 44% pre-strain) were prepared under different deformation conditions but in a way that similar α′-martensite volume fractions were obtained. The fatigue tests were paired with fracture surface analysis. The following conclusions can be drawn from the investigations:

- Re-solidified material (most often in the form of melt droplets) at the melt ejection site of the laser-cut edge is the dominating fatigue crack initiation site independent of the degree of pre-deformation introduced.
- Melt droplets with good bonding to the base material can show partial detachment at high degrees of deformation.
- Partial detachment of melt droplets leads to mesoscopic notch formation, which causes a significant decrease in fatigue strength and can lead to late failures even at load cycles well beyond the classical "durability limit" (formerly defined at 2 mio. cycles).

**Author Contributions:** Conceptualization, A.T.Z., S.C.L.F. and M.Z.; Methodology, A.T.Z., S.S. and S.C.L.F.; Validation, A.T.Z., S.C.L.F. and M.Z.; Formal Analysis, A.T.Z., R.K., S.S. and S.C.L.F.; Investigation, A.T.Z., T.W., S.S., J.F., R.K. and S.C.L.F.; Writing—Original Draft Preparation, A.T.Z.; Writing—Review and Editing, S.C.L.F. and M.Z.; Visualization, A.T.Z., T.W. and J.F.; Supervision, A.W., S.C.L.F. and M.Z.; Project Administration, A.W., S.C.L.F. and M.Z.; Funding Acquisition, A.W. and M.Z. All authors have read and agreed to the published version of the manuscript.

**Funding:** Funded by Deutsche Forschungsgemeinschaft (DFG, German Research Foundation): ZI 1006/15-1—Project-ID 413507401. This work was partially supported by the Fraunhofer Internal Programs under Grant No. Attract 025-601314 awarded to S.C.L. Fischer.

**Data Availability Statement:** The data presented in this study are available on request from the corresponding author.

**Conflicts of Interest:** The authors declare no conflict of interest.

## References

1. Ion, J. Laser Processing of Engineering Materials. In *Principles, Procedure and Industrial Application*, 1st ed.; Hill, J., Ed.; Elsevier: Amsterdam, The Netherlands, 2005.
2. Sharma, A.; Yadava, V. Experimental analysis of Nd-YAG laser cutting of sheet materials—A review. *Opt. Laser Technol.* **2018**, *98*, 264–280. [CrossRef]
3. Lo, K.H.; Shek, C.H.; Lai, J. Recent developments in stainless steels. *Mater. Sci. Eng. R Rep.* **2009**, *65*, 39–104.
4. Davison, R.M.; Laurin, T.R.; Redmond, J.D.; Watanabe, H.; Semchyshen, M. A Review of Worldwide Developments in Stainless Steels. *Materials & Design* **1986**, *7*, 111–119.
5. Davis, J.R. *Stainless Steels*; ASM International: Materials Park, OH, USA, 2010.
6. Olson, G.B.; Cohen, M. A general mechanism of martensitic nucleation: Part I. General concepts and the FCC → HCP transformation. *Metall. Trans. A* **1976**, *7*, 1897–1904.
7. Olson, G.B.; Cohen, M. A general mechanism of martensitic nucleation: Part II. FCC → BCC and other martensitic transformations. *Metall. Trans. A* **1976**, *7*, 1905–1914.
8. Meyrick, G.; Powell, G.W. Phase Transformations in Metals and Alloys. *Annu. Rev. Mater. Sci.* **1973**, *3*, 327–362. [CrossRef]

9. Schramm, R.E.; Reed, R.P. Stacking fault energies of seven commercial austenitic stainless steels. *Metall. Trans. A* **1975**, *6*, 1345–1351. [CrossRef]
10. Angel, T. Formation of Martensite in Austenitic Stainless Steels. Effects of Deformation, Temperature, and Composition. *J. Iron Steel Inst.* **1954**, *177*, 165–174.
11. Shen, Y.F.; Li, X.X.; Sun, X.; Wang, Y.D.; Zuo, L. Twinning and martensite in a 304 austenitic stainless steel. *Mater. Sci. Eng. A* **2012**, *552*, 514–522. [CrossRef]
12. Müller-Bollenhagen, C.; Zimmermann, M.; Christ, H.-J. Very high cycle fatigue behaviour of austenitic stainless steel and the effect of strain-induced martensite. *Int. J. Fatigue* **2010**, *32*, 936–942. [CrossRef]
13. Smaga, M.; Walther, F.; Eifler, D. Deformation-induced martensitic transformation in metastable austenitic steels. *Mater. Sci. Eng. A* **2008**, *483–484*, 394–397. [CrossRef]
14. Krupp, U.; Christ, H.-J.; Lezuo, P.; Maier, H.; Teteruk, R. Influence of carbon concentration on martensitic transformation in metastable austenitic steels under cyclic loading conditions. *Mater. Sci. Eng. A* **2001**, *319–321*, 527–530. [CrossRef]
15. Jadhav, A.; Kumar, S. Laser cutting of AISI 304 material: An experimental investigation on surface roughness. *Adv. Mater. Process. Technol.* **2019**, *5*, 429–437. [CrossRef]
16. Geiger, M.; Bergmann, H.W.; Nuss, R. Laser Cutting Of Steel Sheets. In *Proceedings Volume 1022, Laser Assisted Processing*; Laude, L.D., Rauscher, G.K., Eds.; International Congress on Optical Science and Engineering: Hamburg, Germany, 1988.
17. Meurling, F.; Melander, A.; Linder, J.; Larsson, M. The influence of mechanical and laser cutting on the fatigue strengths of carbon and stainless sheet steels. *Scand. J. Metall.* **2001**, *30*, 309–319. [CrossRef]
18. Mäntyjärvi, K.; Väisänen, A.; Karjalainen, J.A. Cutting method influence on the fatigue resistance of ultra-high-strength steel. *Int. J. Mater. Form.* **2009**, *2*, 547–550. [CrossRef]
19. Pessoa, D.; Grigorescu, A.; Herwig, P.; Wetzig, A.; Zimmermann, M. Influence of Notch Effects Created by Laser Cutting Process on Fatigue Behavior of Metastable Austenitic Stainless Steel. *Procedia Eng.* **2016**, *160*, 175–182. [CrossRef]
20. Wanski, T.; Zeuner, A.T.; Schöne, S.; Herwig, P.; Mahrle, A.; Wetzig, A.; Zimmermann, M. Investigation of the influence of a two-step process chain consisting of laser cutting and subsequent forming on the fatigue behavior of AISI 304. *Int. J. Fatigue* **2022**, *159*, 106779. [CrossRef]
21. Talonen, J.; Aspegren, P.; Hänninen, H. Comparison of different methods for measuring strain induced α-martensite content in austenitic steels. *Mater. Sci. Technol.* **2004**, *20*, 1506–1512. [CrossRef]
22. Das, A.; Sivaprasad, S.; Ghosh, M.; Chakraborti, P.C.; Tarafder, S. Morphologies and characteristics of deformation induced martensite during tensile deformation of 304 LN stainless steel. *Mater. Sci. Eng. A* **2008**, *486*, 283–286. [CrossRef]
23. Hecker, S.S.; Stout, M.G.; Staudhammer, K.P.; Smith, J.L. Effects of Strain State and Strain Rate on Deformation-Induced Transformation in 304 Stainless Steel: Part I. Magnetic Measurements and Mechanical Behavior. *Metall. Trans. A* **1982**, *13*, 619–626. [CrossRef]
24. DIN 50100:2016-12, Fatigue Testing—Performance and Evaluation of Cyclic Tests with Constant Load Amplitude for Metallic Material Specimens and Components. Available online: https://dx.doi.org/10.31030/2580844 (accessed on 20 December 2021).
25. Grigorescu, A.; Hilgendorff, P.M.; Zimmermann, M.; Fritzen, C.P.; Christ, H.J. Effect of Geometry and Distribution of Inclusions on the VHCF Properties of a Metastable Austenitic Stainless Steel. *Adv. Mater. Res.* **2014**, *891–892*, 440–445. [CrossRef]
26. Hilgendorff, P.-M.; Grigorescu, A.C.; Zimmermann, M.; Fritzen, C.-P.; Christ, H.-J. Cyclic deformation behavior of austenitic Cr–Ni-steels in the VHCF regime: Part II—Microstructure-sensitive simulation. *Int. J. Fatigue* **2016**, *93*, 261–271. [CrossRef]
27. Bayerlein, M.; Christ, H.-J.; Mughrabi, H. Plasticity-induced martensitic transformation during cyclic deformation of AISI 304L stainless steel. *Mater. Sci. Eng. A* **1989**, *114*, L11–L16. [CrossRef]
28. Smaga, M.; Boemke, A.; Daniel, T.; Skorupski, R.; Sorich, A.; Beck, T. Fatigue Behavior of Metastable Austenitic Stainless Steels in LCF, HCF and VHCF Regimes at Ambient and Elevated Temperatures. *Metals* **2019**, *9*, 704. [CrossRef]